Gaussian beam based sensitivity kernel calculation and its applications in turning wave tomography

Yu Geng, Modeling and Imaging Lab, IGPP, University of California, Santa Cruz, visiting from Institute of Wave and Information, Xi'an Jiaotong University.*
Xiao-Bi Xie, Modeling and Imaging Lab, IGPP, University of California, Santa Cruz.

Summary

We introduce a Gaussian beam (GB) based method to calculate finite-frequency sensitivity kernels and test its applications in turning wave tomography. The GB summation method has the advantage of high computation efficiency and no any angle limitations. Thus it is suitable in generating sensitivity kernels for high-frequency, long propagation distance and wide-angle waves including the turning waves. We first validate the GB kernels by comparing them with those calculated using analytical and finite-difference (FD) solutions. Then, based on these sensitivity kernels, we build an inversion system for turning-wave travel-time tomography. The proposed method incorporates the wave phenomena into the inversion thus avoids certain difficulties encountered by the high-frequency asymptotic methods. On the other hand, this method still keeps the simplicity of the ray-based tomography method. The preliminary results from numerical tests reveal the potential applications of this method in building velocity models using turning waves.

Introduction

Although velocity tomography and migration velocity updating are traditionally dominated by the ray-based techniques, wave equation based methods gradually gain their ground and are reported to provide better results (Luo and Schuster, 1991; Woodward, 1992; Sava and Biondi, 2004; Spetzler and Snieder, 2004; de Hoop, van der Hilst and Shen, 2006; Jocker et al., 2006; Fliedner and Bevc, 2008). Finite-frequency sensitivity kernels are introduced in velocity tomography to overcome the disadvantage of ray-based method which assumes an infinitely high frequency. Several methods can be used to calculate finite-frequency sensitivity kernels in heterogeneous models (Woodward, 1992; Marquering, Nolet and Dahlen, 1998; Marquering, Dahlen and Nolet, 1999; Dahlen, Hung and Nolet, 2000; Hung, Dahlen and Nolet, 2000; Tian et al., 2007; Xie and Yang, 2008a; Liu et al., 2009).

Turning wave data are widely used to determine the subsurface velocities. Techniques used for this purpose include turning-ray tomography based on the first arrival information (Zhu, Sixta and Angstman, 1992; Stefani, 1995; Bais et al., 2003; Simmons, 2008; Zhu et al., 2008). Recently, following the pioneer works by Lailly (1983) and Tarantola (1984), full-waveform inversion (Pratt and Goulty, 1991; Pratt, 1999; Brenders and Pratt, 2007; Virieux and Operto, 2009) using the entire recorded seismic data, has been increasingly applied in velocity tomography. The full-waveform inversion method usually starts with an initial velocity model which can be estimated from travel-time tomography.

At high-frequencies, wavefield can be described by summation of paraxial GBs (Popov, 1982; Cerveny, 1985), and it has been widely used to construct Green's functions for seismic modeling and imaging (Nowack and Aki, 1984; Hill, 1990; 2001; Gray, 2005; Nowack, 2008; Popov et al., 2010). The GB method overcomes certain critical difficulties such as the two-point boundary value problem and the caustic problem, and can handle wide-angle waves including turning waves. This makes it especially suitable for transmitted wave tomography. The disadvantage of the GB method is that it naturally introduces smooth effects to the obtained wavefield. For very complex models, velocity smoothing is often required, which may limit the applications of the GB method.

Xie (2011) tested using the GB method to calculate finite-frequency sensitivity kernels. In this paper, we continue to discuss the GB based sensitivity kernels and test its applications in turning wave tomography. Compared to the ray tomography, the kernel based method incorporates both wave phenomena and ray concept; while compared to the full-wave equation method, the GB based method is more efficient. In the rest part of this paper, we first discuss how to build finite-frequency sensitivity kernels from GB summation and validate these kernels by comparing them with analytic and FD solutions. We then compare the kernel predicted travel-time delays with those directly measured values. Finally, we create an inversion system using these sensitivity kernels and test turning wave tomography using synthetic data set.

Sensitivity Kernel Calculation and Calibration

The finite-frequency sensitivity kernels for transmitted waves have been discussed by many authors (e.g., Woodward, 1992; Spetzler and Snieder, 2004; Jocker et al., 2006). The frequency domain travel time sensitivity kernel K_F can be expressed as

$$K_F(\mathbf{r},\mathbf{r}_S,\mathbf{r}_G,\omega) = \mathrm{imag}\left[2k_0^2 \frac{G(\mathbf{r};\mathbf{r}_S,\omega)G(\mathbf{r};\mathbf{r}_G,\omega)}{G(\mathbf{r}_G;\mathbf{r}_S,\omega)} \right] \quad (1)$$

where $k_0 = \omega / v_0(\mathbf{r})$ is the background wavenumber, ω is the frequency, $v_0(\mathbf{r})$ is the background velocity, G is the

Green's function, $\mathbf{r}$ is the space location, $\mathbf{r}_S$ and $\mathbf{r}_G$ are the source and receiver locations, and $imag(\cdot)$ denotes taking imaginary part.

The broadband sensitivity kernel can be obtained by stacking single-frequency kernels.

$$K_B(\mathbf{r},\mathbf{r}_S,\mathbf{r}_G) = \int \frac{W(\omega)}{\omega} K_F(\mathbf{r},\mathbf{r}_S,\mathbf{r}_G,\omega) d\omega \ , \quad (2)$$

where

$$W(\omega) = \frac{\omega^2 P(\omega)}{\int \omega^2 P(\omega) d\omega} \quad (3)$$

is the weighting function. $P(\omega) = S(\omega)S^*(\omega)$, and $S(\omega)$ is the source spectrum.

The travel-time difference caused by velocity perturbations can be calculated as

$$\delta t(\mathbf{r}_S,\mathbf{r}_G) = \int \frac{\delta v}{v_0} K_B(\mathbf{r},\mathbf{r}_S,\mathbf{r}_G) dV \ . \quad (4)$$

Equation (4) also forms an integral equation which can be used to invert velocity perturbations $\delta v/v_0$ from travel time residual δt. To validate the GB Green's function and sensitivity kernels, we first compare the analytical, FD and the GB Green's functions. In a 2D homogeneous medium, the Green's function can be calculated using the zeroth-order first-kind Hankel function $H_0^{(1)}(kr)$

$$G(\mathbf{r},\mathbf{r}_S;\omega) = \frac{i}{4} H_0^{(1)}(kr) \ , \quad (5)$$

where $r = |\mathbf{r} - \mathbf{r}_s|$. The asymptotic Green's function can be written as the summation of Gaussian beams $u_{GB}(\mathbf{r},\mathbf{r}_s,\omega)$ over ray parameter θ

$$G(\mathbf{r},\mathbf{r}_S;\omega) \approx \frac{i}{2}\sqrt{\frac{Q_0}{V_0}} \int u_{GB}(\mathbf{r},\mathbf{r}_S,\omega) d\theta \ . \quad (6)$$

Here Gaussian beam $u_{GB}(\mathbf{r},\mathbf{r}_s,\omega)$ can be written in the ray-centered coordinate system as $u(s,n,\omega)$ (Cerveny, Klimes and Psencik, 1984; Nowack and Aki, 1984; Hill, 1990)

$$u(s,n,\omega) = \left[\frac{v(s)}{Q(s)}\right]^{1/2} \exp\left[i\omega\tau(s) + \frac{i\omega}{2}\frac{P(s)}{Q(s)}n^2\right] \ , \quad (7)$$

where s is the coordinate along the ray path, n is the coordinate perpendicular to the ray, τ is the travel time along the ray, and P and Q are complex scalar functions, which can be obtained by solving the dynamic ray tracing equations with initial values $P_0 = i/V_0$ and $Q_0 = \omega_r w_0^2/V_0$. ω_r, w_0 and V_0 stand for reference frequency, the initial beam width and the velocity at the source end of the ray, respectively.

Figure 1 compares the 12 Hz Green's functions calculated using analytical, FD and GB methods, where, except at close to the source, all three methods give almost the same accuracy. We then compare the sensitivity kernels calculated using different methods in a constant velocity model $v_0 = 3.5$ km/s. A 10 Hz Ricker wavelet is used as the source time function and the source-receiver distance is $5\ km$. The sensitivity kernels calculated using different methods are shown in Figure 2. Fifty beams are used to form the GB Green's function, and the initial beam width is $0.58\ km$. The profiles along the two dashed lines in Figure 2 are shown in Figure 3. We see different methods give consistent result. Shown in Figure 4 are comparisons between the FD and GB kernels in a pixel by pixel way, where the vertical and horizontal coordinates are kernel values obtained by using GB and FD methods, respectively. We see most points fall on the unit slope with some scattered points coming from areas close to the source and receiver.

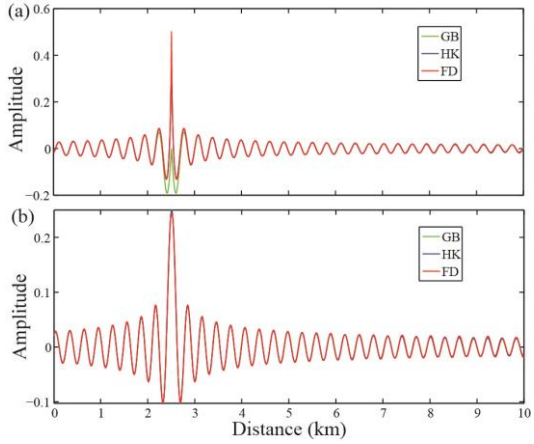

Figure 1: Comarison of 12 Hz Green's function calculated using GB, FD and analytical methods, with (a) real part and (b) imaginary part.

Next, we compare the travel-time differences predicted using the sensitivity kernels with those directly measured. We use a constant background velocity and a Gaussian shaped circular velocity perturbation patch with a radius of $300\ m$ and centered at $x = 4\ km$ and $z = 3.1\ km$. The maximum perturbations at the center of the patch are ranging between -30% and 180%. The predicted travel time difference is calculated using equation (4) with the sensitivity kernel calculated in the background velocity model. The actual travel-time difference is measured from the cross-correlation between synthetic seismograms calculated by FD in the background velocity model and the velocity model including the perturbation. In Figure 5, we plot both values along horizontal and vertical axes. For perturbations between -30% and 60%, the predicted and

measured δt are close to the unit slope. For very large velocity perturbations, the predicted δt show apparent deviations due to the nonlinear effect. However, the predicted δt from kernels calculated using different methods are consistent.

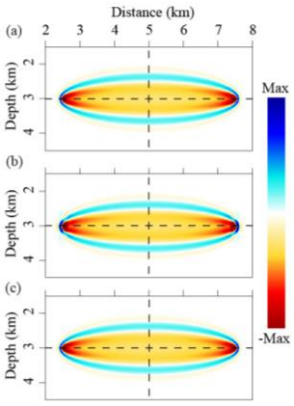

Figure 2: Sensitivity kernels calculated from (a) FD, (b) GB and (c) analytical solutions.

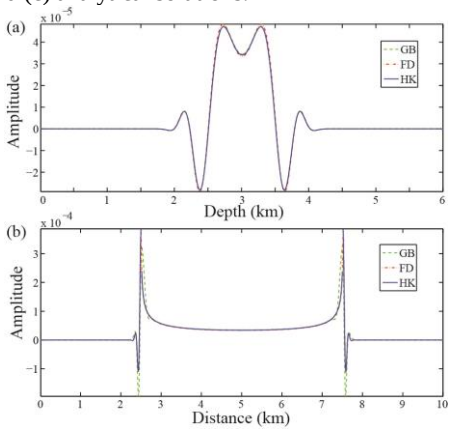

Figure 3: Selected profiles for kernels in Figure 2, (a) along the vertical dashed lines, and (b) along the horizontal dashed lines.

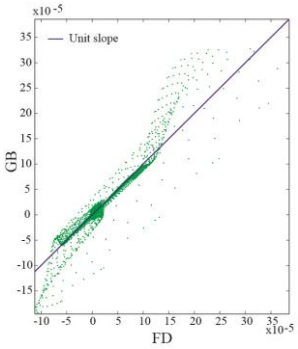

Figure 4: Comparison between the sensitivity kernels caculated using the GB and FD methods.

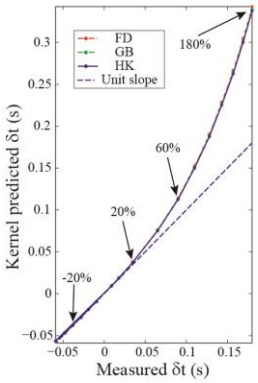

Figure 5: Comparison between the kernel predicted travel time difference δt and directly measured δt.

Inversion System

To build an inversion system, we discretize equation (4) to obtain

$$\delta t(\mathbf{r}_S,\mathbf{r}_G)=\sum_i m(\mathbf{r}_i)K_B(\mathbf{r}_i,\mathbf{r}_S,\mathbf{r}_G)\ , \qquad (8)$$

where both unknown velocity perturbation $m(\mathbf{r}_i)$ and kernel K_B have been partitioned following Xie and Yang (2008b).

Numerical Examples

Resolution test using a checkerboard model. We first test the inversion resolution under the turning wave geometry. As examples, shown in Figure 6 are three broadband turning wave sensitivity kernels calculated in the background model, of which velocities change linearly from $2\ km/s$ at the surface to $3.5\ km/s$ at $3\ km$ depth. The true velocity model (Figure 7a) has a checkerboard shaped perturbation overlapped on the background. The checkerboard has a grid size of $1\ km \times 1\ km$ and the perturbations vary between $\pm 5\%$ (Figure 7b). We use a $10\ Hz$ Ricker wavelet as the source time function. To generate large offset data for inversion, we extend the velocity model on both sides, and use total of 51 shots, each with 28 right-hand side receivers, to illuminate the model. Both the shot and receiver intervals are $0.5\ km$ and the maximum offset is $14\ km$. The background model also serves as the initial model. The travel-time differences are calculated from synthetic data sets generated using the true velocity model and the background velocity. Shown in Figure 7c is the inversion result. Comparing Figures 7c with 7b, the turning wave tomography provides reasonable resolution for the subsurface structures.

Gaussian Beam based sensitivity kernel calculation and its applications in turning wave tomography

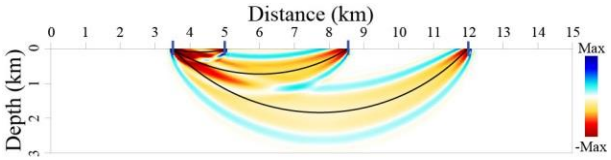

Figure 6: Sensitivity kernels calculated in a model with linear vertical velocity gradient, with offsets 1.5 km, 5.0 km and 8.5 km. Black lines are corresponding geometrical rays.

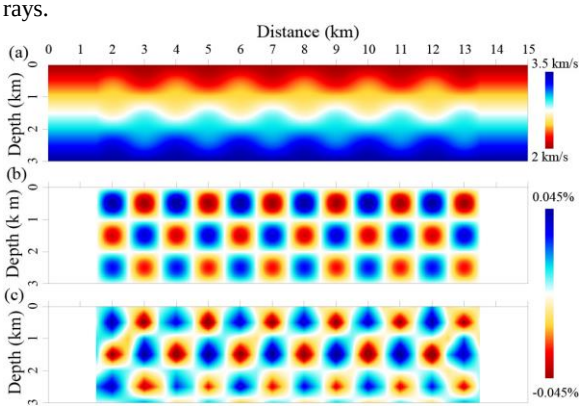

Figure 7: Resolution test using the checkerboard model: (a) true velocity model, (b) velocity perturbations and (c) retrieved perturbations.

Turning wave tomography in a model with high-velocity inclusions. In this example, the true velocity model has a high-velocity patch added to the background velocity, as shown in Figure 9a. The background velocity is similar to that used in the previous example and the patch has a maximum perturbation of 8% (shown in Figure 9b). 10 *Hz* Ricker wavelet is used to generate the synthetic data. For inversion, we use 15 shots and 28 fixed receivers. Both of them are located on the surface between 0.5 *km* to 14.5 *km* , with 1 *km* shot interval and 0.5 *km* receiver interval. The background model also serves as the initial model. In Figure 8, we compare δt values in the data with those predicted by kernels and velocity perturbations. The consistency between two sets of δt values paves the basis for velocity inversion. Shown in Figure 9c is the inversion result. Comparing Figures 9c with 9b, the inverted velocity perturbation reproduces the perturbation pattern with reasonable accuracy. As a preliminary test, iterations are not used in the inversion.

Conclusion

We proposed a method to calculate finite-frequency sensitivity kernels by summing up Gaussian beams. To validate the resulted kernels, we compared the kernel with

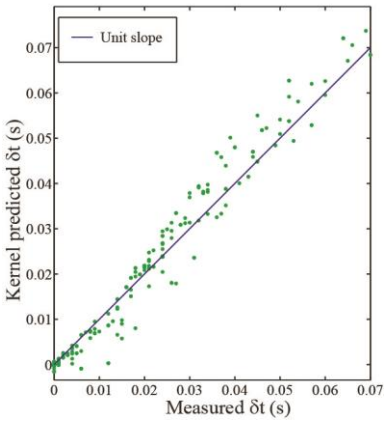

Figure 8: Comparison between the kernel predicted travel time difference and directly measured δt from synthetic data.

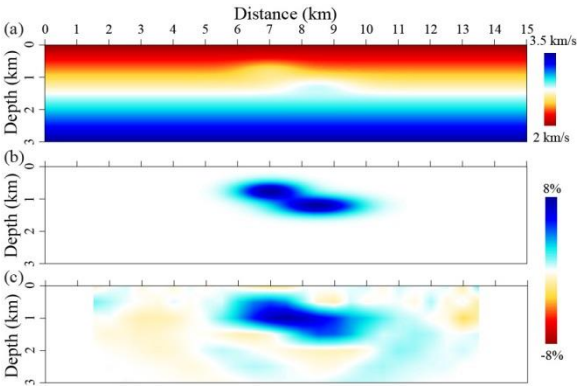

Figure 9: Turning wave tomography result for a model with high-velocity inclusions: (a) true velocity model, (b) velocity perturbations and (c) inverted perturbations.

FD solution and checked the kernel predicted and actually measured travel time residuals. The GB method has the advantage of high computation efficiency and no angle limitation, thus suitable for generating turning wave kernels. We tested the GB kernels in the turning wave tomography and achieved reasonable resolution and accuracy. The velocity tomography based on finite-frequency sensitivity kernels combines the wave phenomena into the inversion but still keeps the simplicity of the ray-based tomography. It is expected that the proposed method will be useful in building velocity models.

Acknowledgment

This research is supported by the WTOPI Research Consortium at the University of California, Santa Cruz. We also thank CWP for ray tracing algorithm in SU.

References

Bais, G., P. P. G. Bruno, V. Di Fiore, and A. Rapolla, 2003, Characterization of shallow volcanoclastic deposits by turning ray seismic tomography: an application to the Naples urban area: J Appl Geophys, **52**, 11-21.

Brenders, A. J., and R. G. Pratt, 2007, Efficient waveform tomography for lithospheric imaging: implications for realistic, two-dimensional acquisition geometries and low-frequency data: Geophys J Int, **168**, 152-170.

Cerveny, V., 1985, Gaussian-Beam Synthetic Seismograms: J Geophys-Z Geophys, **58**, 44-72.

Dahlen, F. A., S. H. Hung, and G. Nolet, 2000, Frechet kernels for finite-frequency traveltimes - I. Theory: Geophys J Int, **141**, 157-174.

de Hoop, M. V., R. D. van der Hilst, and P. Shen, 2006, Wave-equation reflection tomography: annihilators and sensitivity kernels: Geophys J Int, **167**, 1332-1352.

Fliedner, M. M., and D. Bevc, 2008, Automated velocity model building with wavepath tomography: Geophysics, **73**, 195-204.

Gray, S. H., 2005, Gaussian beam migration of common-shot records: Geophysics, **70**, S71-S77.

Hill, N. R., 1990, Gaussian-Beam Migration: Geophysics, **55**, 1416-1428.

---, 2001, Prestack Gaussian-beam depth migration: Geophysics, **66**, 1240-1250.

Hung, S. H., F. A. Dahlen, and G. Nolet, 2000, Frechet kernels for finite-frequency traveltimes - II. Examples: Geophys J Int, **141**, 175-203.

Jocker, J., J. Spetzler, D. Smeulders, and J. Trampert, 2006, Validation of first-order diffraction theory for the traveltimes and amplitudes of propagating waves: Geophysics, **71**, T167-T177.

Lailly, P., 1983, The seismic inverse problem as a sequence of before stack migrations: Expanded Abstracts, Conference on Inverse Scattering, Theory and Application, Society for Industrial and Applied Mathematics, , 206-220.

Liu, Y. Z., L. G. Dong, Y. W. Wang, J. P. Zhu, and Z. T. Ma, 2009, Sensitivity kernels for seismic Fresnel volume tomography: Geophysics, **74**, U35-U46.

Luo, Y., and G. T. Schuster, 1991, Wave-Equation Traveltime Inversion: Geophysics, **56**, 645-653.

Marquering, H., F. A. Dahlen, and G. Nolet, 1999, Three-dimensional sensitivity kernels for finite-frequency traveltimes: the banana-doughnut paradox: Geophys J Int, **137**, 805-815.

Marquering, H., G. Nolet, and F. A. Dahlen, 1998, Three-dimensional waveform sensitivity kernels: Geophys J Int, **132**, 521-534.

Nowack, R., and K. Aki, 1984, The Two-Dimensional Gaussian-Beam Synthetic Method - Testing and Application: J Geophys Res, **89**, 7797-7819.

Nowack, R. L., 2008, Focused Gaussian Beams for Seismic Imaging: Expanded abstracts, SEG 78th Annual Meeting, 2376-2380.

Popov, M. M., 1982, A New Method of Computation of Wave Fields Using Gaussian Beams: Wave Motion, **4**, 85-97.

Popov, M. M., N. M. Semtchenok, P. M. Popov, and A. R. Verdel, 2010, Depth migration by the Gaussian beam summation method: Geophysics, **75**, S81-S93.

Pratt, R. G., 1999, Seismic waveform inversion in the frequency domain, Part 1: Theory and verification in a physical scale model: Geophysics, **64**, 888-901.

Pratt, R. G., and N. R. Goulty, 1991, Combining Wave-Equation Imaging with Traveltime Tomography to Form High-Resolution Images from Crosshole Data: Geophysics, **56**, 208-224.

Sava, P., and B. Biondi, 2004, Wave-equation migration velocity analysis. I. Theory: Geophys Prospect, **52**, 593-606.

Simmons, J. L., 2008, Turning-ray tomography using a low-spatial-frequency model parameterization: Geophysics, **73**, 93-100.

Spetzler, J., and R. Snieder, 2004, The Fresnel volume and transmitted waves: Geophysics, **69**, 653-663.

Stefani, J. P., 1995, Turning-Ray Tomography: Geophysics, **60**, 1917-1929.

Tarantola, A., 1984, Inversion of Seismic-Reflection Data in the Acoustic Approximation: Geophysics, **49**, 1259-1266.

Tian, Y., R. Montelli, G. Nolet, and F. A. Dahlen, 2007, Computing traveltime and amplitude sensitivity kernels in finite-frequency tomography: J Comput Phys, **226**, 2271-2288.

Virieux, J., and S. Operto, 2009, An overview of full-waveform inversion in exploration geophysics: Geophysics, **74**, Wcc1-Wcc26.

Woodward, M. J., 1992, Wave-Equation Tomography: Geophysics, **57**, 15-26.

Xie, X. B., 2011, Calculating finite-frequency sensitivity kernels using the Gaussian beam method: Expanded abstracts, SEG 81th Annual Meeting, **30**, 3892-3897.

Xie, X. B., and H. Yang, 2008a, The finite-frequency sensitivity kernel for migration residual moveout and its applications in migration velocity analysis: Geophysics, **73**, S241-S249.

---, 2008b, A wave-equation migration velocity analysis approach based on the finite-frequency sensitivity kernel: Expanded abstracts, SEG 78th Annual Meeting, **27**, 3093-3097.

Zhu, X. H., D. P. Sixta, and B. G. Angstman, 1992, Tomostatics; turning-ray tomography + static corrections The Leading Edge, **11**, 15-23.

Zhu, X. H., P. Valasek, B. Roy, S. Shaw, J. Howell, S. Whitney, N. D. Whitmore, and P. Anno, 2008, Recent applications of turning-ray tomography: Geophysics, **73**, 243-254.